



## Assessing the impact of landwater on the Northwest Pacific using normalized Total Alkalinity

Tatsuki Tokoro<sup>1, 6</sup>, Shin-Ichiro Nakaoka<sup>1</sup>, Shintaro Takao<sup>1</sup>, Shu Saito<sup>2</sup>, Daisuke Sasano<sup>3</sup>, Kazutaka Enyo<sup>3</sup>, Masao Ishii<sup>4</sup>, Naohiro Kosugi<sup>4</sup>, Tsuneo Ono<sup>5</sup>, Kazuaki Tadokoro<sup>5</sup>, and Yukihiko Nojiri<sup>1</sup>

<sup>1</sup>formaly at: Earth System Division, National Institute for Environmental Studies, Tsukuba, Japan.

<sup>2</sup>Administration Department, Japan Meteorological Agency, Tokyo, Japan.

<sup>3</sup>Atmosphere and Ocean Department, Japan Meteorological Agency, Tokyo, Japan.

<sup>4</sup>Department of Climate and Geochemistry Research, Meteorological Research Institute, Tsukuba, Japan.

10 <sup>5</sup>Fisheries Resources Institute, Japan Fisheries Research and Education Agency, Yokohama/Shiogama, Japan.

<sup>6</sup>currently at: Seto Inland Carbon-Neutral Research Center, Hiroshima University, Hiroshima, Japan.

Corresponding author: Tatsuki Tokoro (tokorota@hiroshima-u.ac.jp, tokoro.tatsuki@nies.go.jp)

**Abstract.** The impact of landwater was assessed using salinity-normalized Total Alkalinity observations. The observational data included surface carbonate parameters from decades of surveys conducted by volunteer cargo ships and research vessels in the Northwest Pacific. Statistical processes, such as re-gridding and Fourier regression, used in a previous study were also applied in this study to improve the spatiotemporal resolution. First, the seawater area affected by landwater was identified using an Empirical Orthogonal Function analysis of normalized Total Alkalinity. The differences in normalized Total Alkalinity and Dissolved Inorganic Carbon from the surrounding area were then analysed to evaluate the causes such as landwater supply, advection effects, and biological activities. In addition, the impact of landwater on oceanic CO<sub>2</sub> uptake and acidification in the study area was assessed. The analysis showed that landwater was the main source of total coastal Alkalinity but was not the dominant cause of Dissolved Inorganic Carbon. The supply of landwater had little effect on oceanic CO<sub>2</sub> uptake throughout the year. The supply of by landwater was a factor in coastal acidification; however, the supplied Total Alkalinity reduced the overall acidification trend by 65%. The results of this study are expected to be further improved by enhancing observations, such as the vertical profiles of carbonate parameters, and are expected to expand to other sea areas and be applied to global budgets.



## 1. Introduction

The flow of landwater to the ocean is one of the most important flows in the Earth's system. In the carbon cycle, landwater is the major carbon source for the oceans (Aufdenkampe et al., 2011; Bauer et al., 2013; Borges et al., 2005; Cai, 2011; Chen and Borges, 2009; Chen et al., 2013), which is responsible for atmospheric CO<sub>2</sub> emissions and acidification in coastal areas  
35 (Carstensen and Durate, 2019; Duarte et al., 2013; Tranvik et al., 2009). However, strong carbon flows, such as biological pumps, impact carbonate distribution in coastal areas (Passow and Carlson, 2012; Regnier et al., 2013, 2022). Quantifying these complex flows is important for predicting future climate change and ocean acidification as well as for predicting biochemical changes in coastal areas. The Northwest Pacific Ocean, including the coastal areas of Japan, is one of the strongest sinks of atmospheric CO<sub>2</sub> (Takahashi et al., 2002, 2009). Therefore, it is crucial to assess the impacts of landwater  
40 on oceanic CO<sub>2</sub> uptake and coastal acidification.

While several studies on carbonate systems have been conducted in the Northwest Pacific Ocean (e.g., Ishii et al., 2001; Murata et al., 1998; Takamura et al., 2010; Tokoro et al., 2023; Yoshikawa-Inoue et al., 1995, 2014), spatiotemporal variations in landwater in seas in this region have not yet been quantified. Landwater tracers are one of the most effective methods for evaluating the influence of landwater. Although salinity is the most frequently assessed factor in land-water  
45 transportation, other factors such as precipitation and evaporation also impact this transportation. This omission can be source of major error in the assessment of land-water transportation in the northwestern Pacific region, where high precipitation and evaporation by low-pressure systems and heat waves, respectively, have been observed (Kitamura et al., 2016; Miyama et al., 2021; Sugimoto et al., 2013).

The total Alkalinity (TA) normalized by salinity is a potential indicator to assess the influence of landwater on ocean. TA is a carbonate parameter in seawater and is defined by the charge balance of dissolved ions, such as hydrogen carbonate (Zeebe and Wolf-Gladrow, 2001). TA depends on several factors, such as advection from different water masses and biological metabolism, including the calcification and dissolution of calcium carbonate (e.g., Broecker and Peng, 1982; Lee et al., 2006; Millero et al., 1998). TA is also highly correlated with salinity; however, TA normalized to the reference salinity (nTA) has been used to quantify the above factors. nTA is calculated as follows:

$$55 \quad nTA = TA \cdot \frac{S_{ref}}{S} \quad (1)$$

where,  $S$  and  $S_{ref}$  are the measured and reference salinities (traditionally 35), respectively. Similarly, Dissolved Inorganic Carbon concentration (DIC) was also normalized (nDIC). Equation (1) is formulated based on the assumption that a water mass with zero salinity has zero TA. However, this assumption is not true for landwater because its TA is greater than zero, even when salinity is zero, owing to the weathering of carbonate and silicate rocks (e.g., Friis et al., 2003; Lehmann et al.,  
60 2023; Rassmann et al., 2016; Taguchi et al., 2009). Therefore, when Equation (1) is applied to areas affected by landwater, the nTA value is higher than that of the surrounding seawater. Conversely, the influence of landwater, along with factors such as water mass advection and biological metabolism, can be quantified by assessing the distribution of nTA. Unlike other methods that use salinity as a tracer for landwater, nTA defined in Equation (1) excludes the effect of precipitation and



65 evaporation, which is advantageous because contamination by water masses with almost zero salinity and TA can be excluded. It is also easier to quantify the influence of seawater from different local areas because the TA has different values in different local areas, even if the salinity is the same (Lee et al., 2006; Takatani et al., 2014).

In this study, we aimed to analyse the influence of landwater on carbonate systems in the ocean using nTA and other carbonate parameters measured by voluntary cargo ships and research vessels in the Northwest Pacific. First, spatiotemporal variations in the area in which landwater significantly affected surface seawater were identified using Empirical Orthogonal Function (EOF) analysis of the nTA distribution. Second, we focused on the differences in TA and DIC between the landwater-affected area and surrounding areas and quantified the landwater supply and other contributing factors that affect TA and DIC. The final step involved the evaluation of the effects of landwater on the environment. Seawater CO<sub>2</sub> fugacity (fCO<sub>2</sub>) and the calcite saturation state of seawater ( $\Omega_{\text{cal}}$ ) were the two carbonate parameters that were used as the index of environmental changes caused by landwater input. The former parameter affects the sea CO<sub>2</sub> flux. The TA and DIC supplied by landwater should change seawater fCO<sub>2</sub> and oceanic CO<sub>2</sub> uptake. Meanwhile,  $\Omega_{\text{cal}}$  is the ratio of the concentration product of [Ca<sup>2+</sup>] and [CO<sub>3</sub><sup>2-</sup>] to the solubility product of calcite and is an index of ocean acidification. In coastal areas, the decomposition of organic matter supplied by landwater is expected to cause more severe acidification, which may cause harmful algal growth and adversely affect marine products such as bivalves (Fitzer et al., 2018; Kessouri et al., 2021; Wallace et al., 2014). Therefore, the analysis of changing  $\Omega_{\text{cal}}$  is expected to lead to a more detailed assessment of coastal acidification. This study also aimed to evaluate the effects of landwater on future climate change and coastal acidification and to predict the effects of future environmental changes.

## 2. Methods

### 2.1 Data for analysis

85 The observational data in this study were collected by the National Institute for Environmental Studies (NIES), Meteorological Research Institute (MRI) of the Japan Meteorological Agency (JMA), and Japan Fisheries Research and Education Agency (FREA). The NIES data were produced as part of the Voluntary Observing Ship (VOS) programs for cargo ships (namely, M/S Alligator Hope, M/S Pyxis, M/S New Century 2, and M/S Trans Future 5). MRI, JMA, and FREA collected data from research vessels (R/V Mirai and R/V Hakuho-maru for MRI; R/V Keifu-maru and R/V Ryofu-maru for JMA; and R/V Wakataka-maru and R/V Soyo-maru for FREA). These data were uploaded to the Surface Ocean CO<sub>2</sub> Atlas (SOCAT; Pfeil et al., 2013; Bakker et al., 2016, <https://socat.info/index.php/data-access/>) and Global Ocean Data Analysis Project (GLODAP, Key et al., 2015; Olsen et al., 2016; Olsen et al., 2020, <https://glodap.info/>). These observations were statistically processed by re-gridding, a second-order approximation of TA, carbonate equilibrium calculations, and Fourier regression into datasets with a spatial resolution of 1° × 1° and a temporal resolution of 0.1 year, as suggested in a previous study (Tokoro et al., 2023). Similar to the previous study, the data was excluded from the analysis if there was insufficient



temporal data ( $n \geq 60$ ) in the  $1^\circ \times 1^\circ$  spatial grid. Although the time interval (from January 1, 2000, to December 31, 2019), covered area (latitudes of  $20\text{--}50^\circ\text{N}$  and longitudes of  $120\text{--}160^\circ\text{E}$ ), and original observations in the SOCAT by NIES were the same as those in the previous study, the original observations by MRI and JMA increased slightly (287750 to 291138) with the upgrade of the product (SOCAT ver. 2019 to 2023). The FREA dataset is a new addition to those used in previous studies. As the FREA data ( $n = 566175$ ) were collected every 1 minute while the other data were collected every 10 min, the FREA data were weighted 1/10 with respect to the other data and weighted averaged as the gridded data. The GLODAP data for surface ( $<10$  m depth) TA and DIC from the MRI and JMA were updated using ver. 2.2020 to 2.2023. The number of data points for JMA data increased from 2080 to 2163. However, the effect of increase in the data was small, which did not statistically affect the result (Table S1). Additionally, observations up to a depth of 150 m within the GLODAP were used to evaluate the effects of vertical advection (Text S1).

## 2.2 EOF analysis, Cause Analysis, and Environmental Impact Assessment

In this study, areas significantly affected by landwater were identified by applying EOF analysis to the spatiotemporal variability of nTA. The EOF analysis breaks down spatiotemporal variations into multiple orthogonal modes with multiple spatial patterns (principal EOF patterns) and time series (principal component time series) (e.g., Denbo and Allen, 1984). Using the principal EOF pattern and principal component time series with respect to the spatiotemporal variation of nTA, we identified that “Area A” was significantly influenced by landwater. Thereafter, we labelled the surrounding area as “Area B.” The influence of landwater was quantified as the value of Area A minus that of Area B ( $dAB$ ).

Causal analysis of  $dAB$  of TA and DIC was performed using the following equation:

$$\frac{\partial dAB}{\partial t} = Sup_{lw} + C_{flux} + C_{res} \quad (2)$$

The left-hand side of the equation represents the time derivative of  $dAB$  of TA and DIC, calculated from the normalized values (nTA and nDIC, respectively) to exclude the effect of seawater volume change due to landwater inflow.  $Sup_{lw}$  is the TA or DIC supply by landwater;  $C_{flux}$  is the term of difference in air-sea  $\text{CO}_2$  flux between Areas A and B divided by  $MLD$ , which is the mixed layer depth calculated from the reanalysis data of seawater temperature profiles by Japan Agency for Marine-Earth Science and Technology (JCOPE2M; Miyazawa et al., 2017, 2019, <https://www.jamstec.go.jp/jcope/htdocs/distribution/>) as isothermal depth at  $\Delta T = 0.2^\circ\text{C}$  with linear interpolation (de Boyer Montégut et al., 2004; Holte and Talley, 2009); this term was applied only to the DIC input.  $C_{res}$  is the TA or DIC input due to other residual factors related to  $dAB$  (e.g., horizontal and vertical advection and biological metabolism).

$Sup_{lw}$  was estimated from river discharge and TA or DIC in river water as follows:

$$Sup_{lw} = \frac{Flow_r \cdot C_r}{MLD \cdot A} \quad (3)$$

where,  $Flow_r$  is the monthly total flow rate of the river,  $C_r$  represents the TA or DIC of the associated rivers,  $A$  is the area of Area A. The flow rate was estimated using the Water Information System database of the Ministry of Land, Infrastructure,



Transport, and Tourism of Japan (<http://www1.river.go.jp/>). As TA and DIC data were not available for all rivers, the referential values for zero-salinity endmembers in the three most river-influenced inner bays (Tokyo Bay, Ise Bay, and Osaka Bay) in the relevant coastal areas were used (518–1006 and 475–1371  $\mu\text{mol kg}^{-1}$  for TA and DIC, respectively; Taguchi et al., 2009; Tokoro et al., 2021). Notably, TA range did not consider seasonal variations; however, the effect of spatial differences among the three bays was more pronounced. All data were regrided to the resolution of the processed SOCAT and GLODAP data (spatial and temporal resolution of  $1^\circ \times 1^\circ$  and 0.1 year, respectively).

Air-sea  $\text{CO}_2$  flux was determined by the air-sea  $\text{fCO}_2$  difference between Areas A and B, which was calculated from the processed  $\text{fCO}_2$  data and wind velocity from the database of the Cross-Calibrated Multi-Platform (CCMP, Atlas et al., 2011; Mears et al., 2019, <https://data.remss.com/ccmp/v02.0/>, version 2.0). The details of the calculations are the same as those used in a previous study (Tokoro et al., 2023).

The effect of landwater on air-sea  $\text{CO}_2$  flux and acidification were quantified by multivariate analysis using *dAB* of seawater  $\text{fCO}_2$  and  $\Omega_{\text{cal}}$  as the objective variables and *dAB* of SST (Sea Surface Temperature), SSS (Sea Surface Salinity), nTA, and nDIC as the explanatory variables. Although both seawater  $\text{fCO}_2$  and  $\Omega_{\text{cal}}$  can be unambiguously determined from equilibrium calculation using SST, SSS, nTA, and nDIC (Zeebe and Wolf-Gladrow, 2001), a multivariate linear model should be useful because these have a non-linear relationship, and it is difficult to intuitively understand the contribution of the explanatory variables. Partial least squares regression (PLS regression; Wold et al., 2001) was used in the multivariate analysis to prevent multicollinearity, especially considering the strong correlation between SSS and nTA and nDIC.

### 145 3. Results

Figure 1 represents the processed spatial distributions of SSS, TA, and nTA. The SSS showed a north-south gradient, which was attributed to freshwater inflow from the Amur River in the north and high evaporation at horse latitudes. There was also an area of reduced SSS along the Pacific coast of mainland Japan (32–34°N, 132–140°E; Figure 1a). These trends were similar for TA, which exhibited high correlation with SSS ( $R^2 = 0.94$ ) (Figure 1b). The nTA was high in the northern part of the study area, and slightly high values were also observed along the Pacific coast of Japan (Figure 1c). The intercept of the regression line between SSS and TA was  $528.04 \pm 2.00 \mu\text{mol kg}^{-1}$  (Ave  $\pm$  SE), which was consistent with the TA value of the Amur River ( $589 \mu\text{mol kg}^{-1}$ ; Andreev and Pavlova, 2009) and Japanese river water ( $518\text{--}1006 \mu\text{mol kg}^{-1}$ ) (Figure 1d). In contrast, nTA was inversely proportional to SSS ( $R^2 = 0.57$ ), with a lower SSS tending to have a higher nTA (Figure 1e). These results indicate that the study area was affected by freshwater with TA above zero, especially in the northern area and on the Pacific coast of Japan.

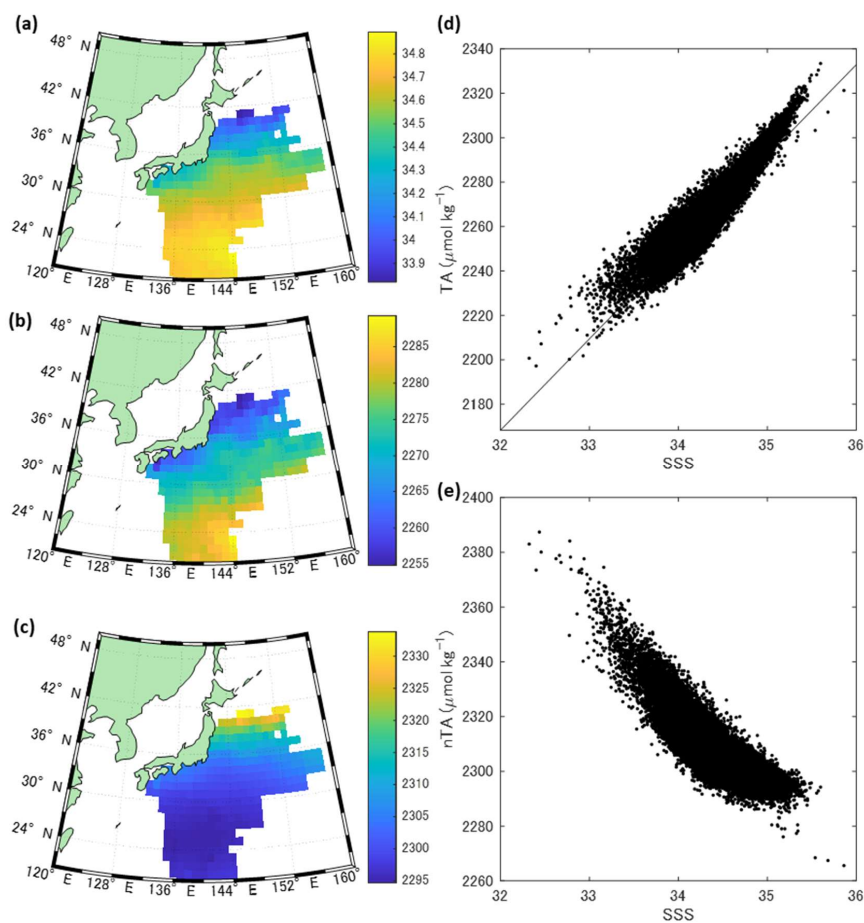
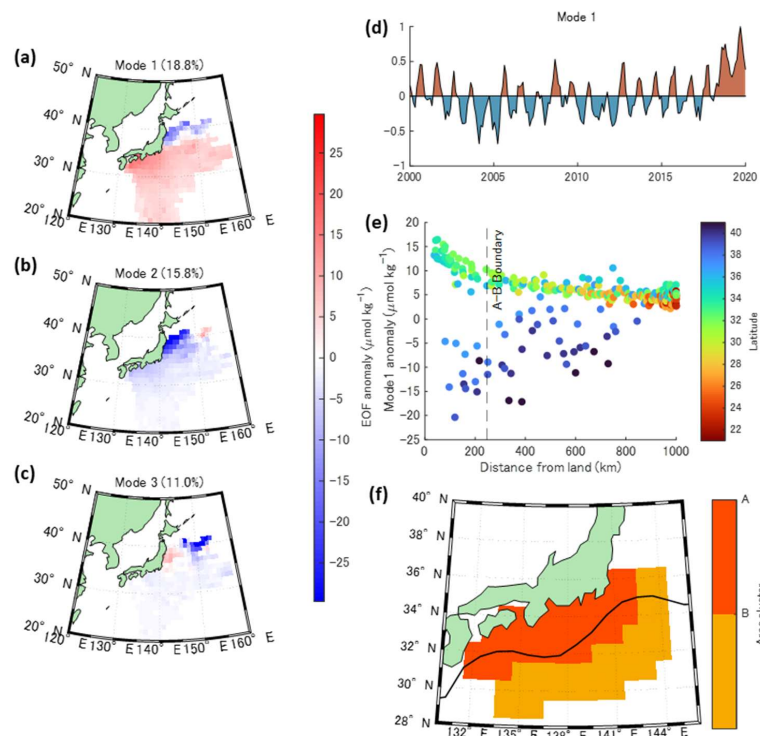


**Figure 1 (a–c):** Spatial distribution of (a) mean SSS (b) TA and (c) nTA. (d and e): Scatterplot of (d) SSS-TA and (e) SSS-nTA. The black line is the approximate line ( $R^2 = 0.94$ ,  $TA = (50.46 \pm 0.06) \times SSS + (528.04 \pm 2.00)$  (Ave.  $\pm$  SE)).

160 The spatial distribution of nTA in the three most dominant modes of the EOF analysis is shown in Figure 2(a–c). The principal EOF patterns were indicated by a parameter defined as “EOF anomaly,” denoted by red or blue in Figure 2. The



spatiotemporal variation of the nTA anomaly in each mode was expressed as the product of the EOF anomaly and the principal component time series. In the most dominant mode (Mode 1), the principal patterns exhibited a clear north-south difference at approximately 37°N (Figure 2a). The principal component of the time series in Mode 1 (Figure 2d) indicated  
165 that the annual cycle was predominant, and maximum nTA was observed in summer south of 37°N, whereas the maximum was in winter north of 37°N (data not shown). The seasonal variation south of 37°N can be explained by the fact that landwater supply is proportional to the precipitation over land, thereby reaching its peak in summer on the Pacific side of Japan. For the area north of 37°N, this may be due to the southward transportation of high-nTA surface seawater in the Pacific subarctic region by northerly winds in winter or winter vertical mixing that supplied subsurface high-nTA seawater  
170 to the surface. In addition, the EOF anomaly south of 37°N was significantly correlated with distance from the Japanese mainland (Figure 2e). The degree of temporal variation in nTA, as shown in Figure 2d, increased significantly closer to mainland Japan in this mode. The other major modes (Modes 2 and 3; Figure 2b, c) had an east-west distribution north of 37°N. A distribution such as this could represent seasonal or multi-year variations in the flow path of the Kuroshio Extension. Based on the above considerations, we determined that it was appropriate to use the Mode 1 EOF anomaly south of 37°N as  
175 an indicator of the influence of landwater from mainland Japan. Although the area north of 37°N contains Japanese rivers with large flow rates (e.g., the Kitakami River), the effect of landwater was excluded from the analysis in this study because the influence of high nTA in the subarctic gyre was too dominant to extract the influence of landwater from Japan. The influence of subarctic Pacific seawater can be expected even around 37°N; however, this is not expected to have a significant effect on the statistics in Area A, such as the spatial mean values. Area A is located south of 37°N and within 246.67 km of  
180 land (Figure 2f). This distance is defined using change-point detection (Killick et al., 2012), meaning that the mean EOF anomaly south of 37°N changes abruptly before and after this distance. The outer edge of Area A roughly aligned with the Kuroshio axis, as indicated by the JCOPE2 SSH data (SSH = 0.2 m). Although the EOF anomaly outside Area A also shows a relatively weak correlation with distance, this correlation is thought to be due to the influence of landwater from areas other than Japan, such as East Asia, which was difficult to quantify using the measurement data in this study. To minimize  
185 the influence of landwater outside Japan and differences in latitude and longitude, Area B was determined as adjacent to Area A, similar in size to the area for comparison (Figure 2f).



190 **Figure 2.** (a–c): EOF anomaly of (a) Mode 1, (b) Mode 2, and (c) Mode 3. The percentage in the bracket (18.8%) indicates the contribution of this mode to the original variation. (d): Principal component of time series of Mode 1. (e): Scatterplot of EOF anomaly of Mode 1 versus distance from Japan mainland. The plot colours indicate the latitude. The dotted line represents the boundary of Areas A and B estimated using the changepoint analysis. (f): Distribution of Area A and B. The black curve indicates mean Kuroshio axis during the whole period in this study (2000–2019).

195 The monthly and annual average values of the differences in the relevant parameters (SST, SSS, nTA, and nDIC) between Areas A and B ( $dAB$ ) are shown in Figure 3. All  $dAB$  parameters showed seasonal variation, and the absolute values of  $dAB$  were largest in winter for SST and nDIC and in summer for SSS and nTA. On a decadal scale, the absolute values of all  $dAB$  tended to increase significantly. This indicates that the supply of landwater increased, which was consistent with the fact that precipitation in relevant areas in Japan was reported to have been increasing during the period analysed in this study by the  
 200 Japan Meteorological Agency (<https://www.data.jma.go.jp/cpd/cgi-bin/view/index.php>).



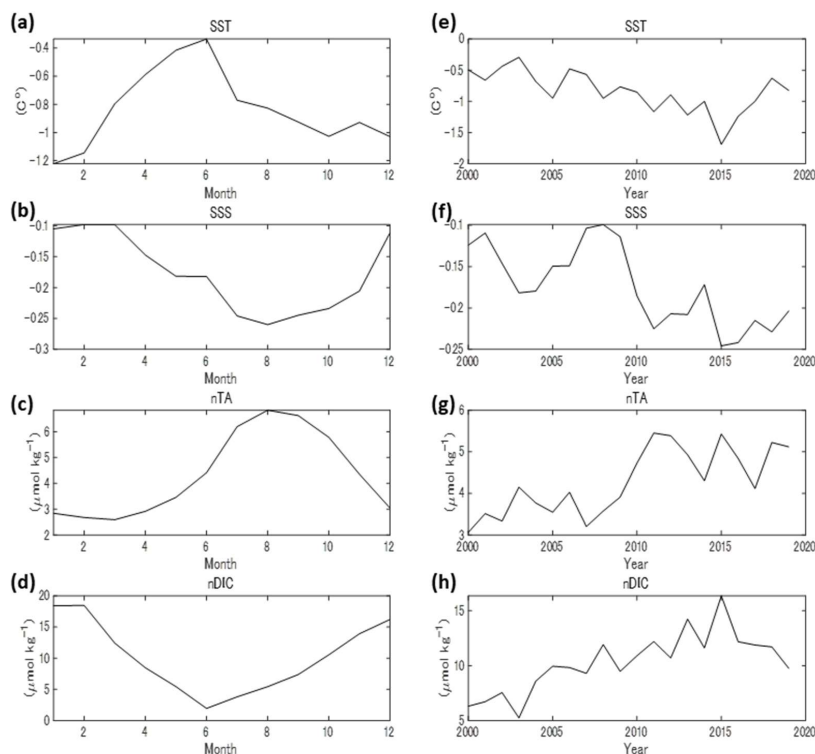
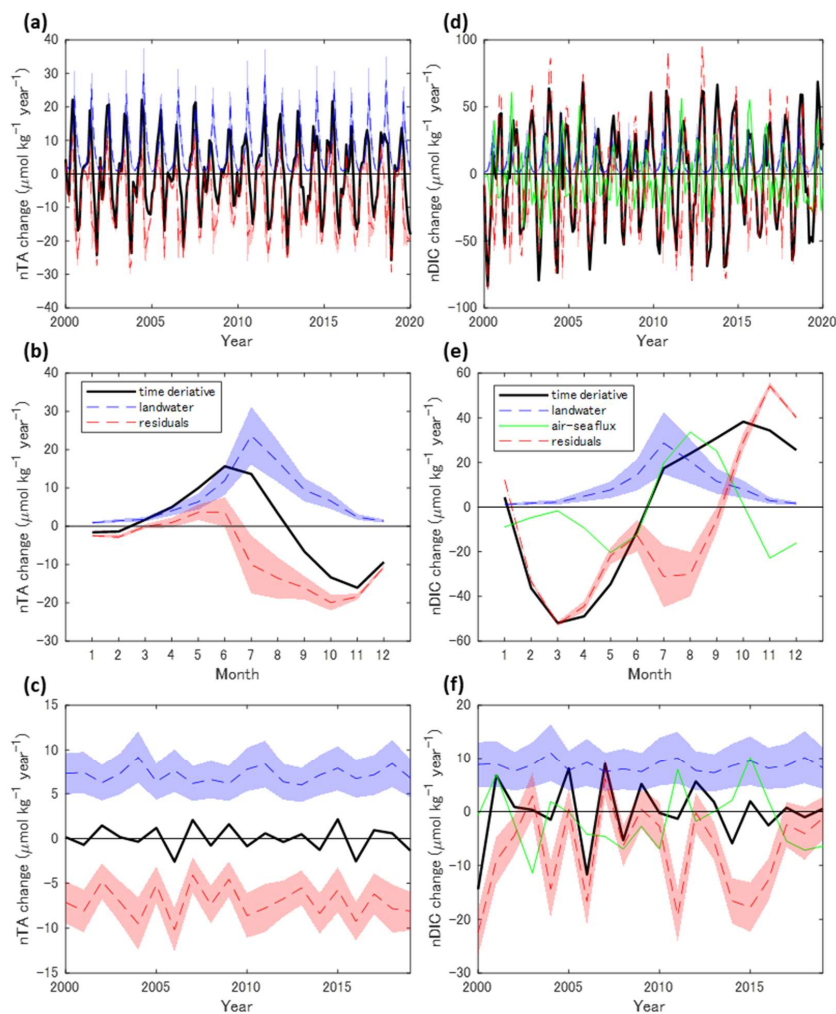


**Figure 3.** The differences in SST, SSS, nTA, and nDIC between Areas A and B (*dAB*). (a)–(d): Seasonal variations. (e)–(h): Annual variations. Although the time step in this study was 0.1 year, the monthly values were calculated by spline interpolation of values at 1/12-year intervals. The same applies to the other figures.

Figure 4 represents the time-series variations of each term in Equation (2) used for the causal analysis of the *dAB* of nTA and nDIC. The river discharge for  $Sup_{hw}$  was calculated as the sum of the 37 rivers bordering Area A (see Text S2). The maximum nTA and nDIC  $Sup_{hw}$  were observed during the summer months, when precipitation on the Pacific coast of Japan was the highest. Though the air-sea CO<sub>2</sub> flux term ( $C_{flux}$ ) also showed a clear seasonal variation, the annual average did not. The residual term ( $C_{res}$ ) tended to be negative for both TA and DIC; however, the seasonal patterns and ranges of variation differed considerably.

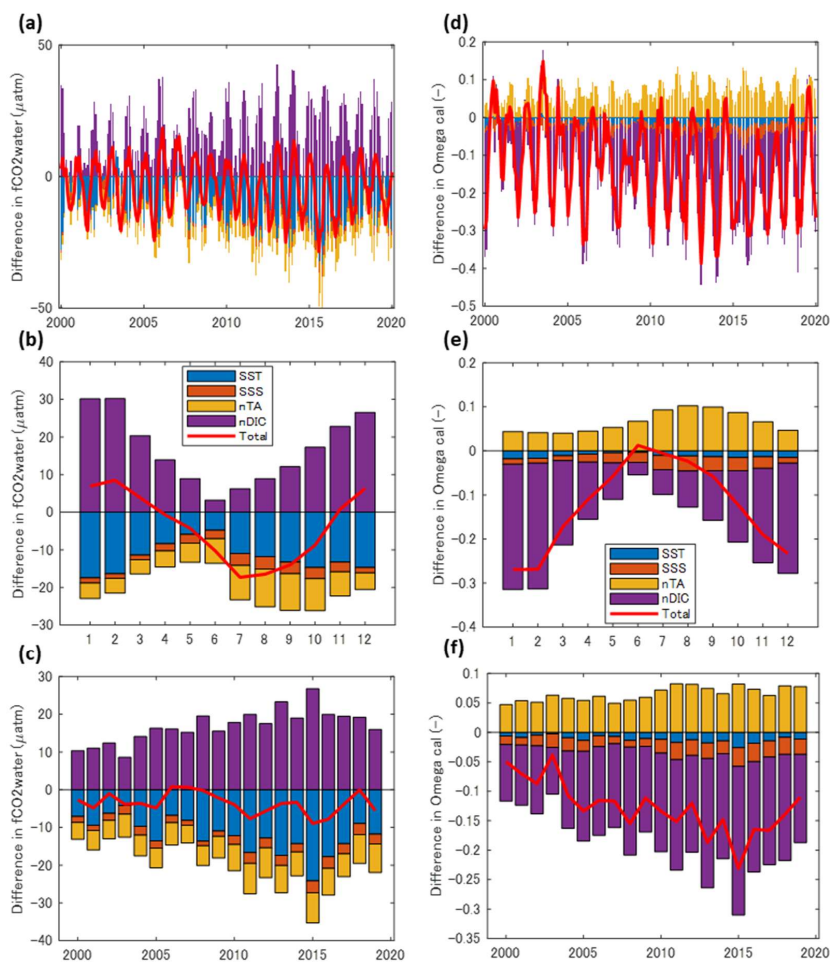


215 **Figure 4.** (a): Temporal variations of nTA time derivative and related terms in Equation (2). (b): The monthly averages. (c): The yearly averages. (d)–(f): Similarly, but for nDIC. The shaded areas are error ranges calculated from the upper and lower limits of the TA ( $518\text{--}1006\ \mu\text{mol kg}^{-1}$ ) for and DIC ( $475\text{--}1371\ \mu\text{mol kg}^{-1}$ ) in landwater. The ranges are not random errors thus have remained the same error range for monthly or yearly averaging. The dotted lines in shaded areas represent the average values.



220 The PLS regression showed that the explanatory variables SST, SSS, nTA, and nDIC explained well the objective variables seawater  $f\text{CO}_2$  ( $r^2 = 0.996$ ) and  $\Omega_{\text{cal}}$  ( $r^2 = 0.997$ ) (Figure 5). The average contributions due to each explanatory variable in the PLS analysis were consistent with those in the equilibrium calculation for seawater  $f\text{CO}_2$  and  $\Omega_{\text{cal}}$  using the averages in Area B and the respective  $dAB$  values (Table S2). Area A had lower seawater  $f\text{CO}_2$  and  $\Omega_{\text{cal}}$  than Area B and both seawater  $f\text{CO}_2$  and  $\Omega_{\text{cal}}$  showed clear seasonal variations.

225





235 **Figures 5. (a): Temporal contributions in the PLS analysis by SST, SSS, nTA, and nDIC to the difference in seawater  $fCO_2$  between Area A and B. (b): The corresponding monthly averages. (c): The corresponding yearly averages. (d): Temporal contributions in the PLS analysis by SST, SSS, nTA, and nDIC to the difference in  $\Omega_{cat}$  between Area A and B. (e): The monthly averages. (f): The yearly averages. . The red lines represent the sum of each contribution and is almost equal to temporal variation of  $dAB$  of seawater  $fCO_2$  and  $\Omega_{cat}$ .**

#### 4. Discussion

235 The extent of Area A defined using nTA (Figure 2f) was consistent with the low-salinity area of the Pacific coast of Japan (Figure 1a). The SSS south of 37°N exhibited an abrupt change in value 205.74 km from mainland Japan (Figure S4), which is consistent with the distance of the boundary between Areas A and B (246.67 km). SSS is affected by precipitation and evaporation; therefore, nTA was a more accurate indicator of landwater than SSS. However, the consistency between the two results provides strong evidence that the nTA in Area A was derived from landwater. These distances were calculated  
240 statistically using 20 years of observational data on SSS and nTA. It would be challenging to obtain a similarly significant result from single observations. Therefore, the findings of this study, which quantify the extent of the influence of landwater, are novel and offer new insights.

To evaluate the effect of the Kuroshio Current on landwater distribution, another EOF analysis was performed using data from the Kuroshio Large Meander period (2017–2020 in this study) in which the Kuroshio path followed an alternative  
245 meandering path south of its usual course (Kawabe, 1985). Area A was within the range of 353.61 km from land, utilizing the Mode 1 EOF anomaly during the meander period, whereas it was 246.67 km during the entire period. This result was consistent with the observed Kuroshio meandering path and supports the assumption that the Kuroshio Current defines Area A. However, Area A extended further out of the open ocean than the Kuroshio axis during the entire study period (Figure 2f). Therefore, the Kuroshio Current limited the spread of landwater to some extent but did not completely inhibit it.

250 The supply of TA by landwater was higher than the time deviation of  $dAB$  for almost the entire period, suggesting that the supply was one of the main factors contributing to the increase in  $dAB$  (Figure 4). On the other hand, the annual rate of increase in the  $dAB$  of nTA was almost zero ( $-0.02 \pm 0.05 \mu\text{mol kg}^{-1} \text{ year}^{-1}$ ). Therefore, the residual term would be the negative value of the same scale with  $Sup_{lw}$  term for TA. The primary cause of the negative residual term is assumed to be horizontal advection. The advection effect can be estimated from the product of the current velocity and  $dAB$  of nTA. The  
255 period of increasing  $dAB$  of nTA (Figure 3c) is consistent with the period of increasing absolute value of the residual term in Figure 4b. In addition, vertical advection could not be the main cause of the negative residual term, because the vertical gradient for calculating vertical advection was small and insignificant (see Text S1). Other causes of the residual term are differences in biological metabolism, such as calcification and nitrate consumption; calcification by coccolithophores is the most promising process for changing oceanic nTA. However, no regional difference in calcification rate of up to  $10 \mu\text{mol kg}^{-1}$



260 <sup>1</sup> year<sup>-1</sup> (Figure 4b) has not been reported between the Japanese coastal Area A (Area A) and the surrounding sea area (Area B) (Hopkins and Balch, 2018; Krumhardt et al., 2019). Another component of TA include nitrate, which is consumed during photosynthesis to raise nTA (Brewer and Goldman, 1976). The data on total nitrate (TN) concentration is available in GLODAP, and the mean values were  $1.19 \pm 0.11 \mu\text{mol kg}^{-1}$  and  $0.34 \pm 0.04 \mu\text{mol kg}^{-1}$  in Area A and B, respectively. As the monthly difference were largest in the winter ( $2.11 \mu\text{mol kg}^{-1}$ ) and almost reach zero in the summer, the main source of  
 265 nitrate would be vertical advection rather than input from land. Nonetheless, the effect of nitrate on TA was probably one order of magnitude smaller than that of the landwater supply and is negligible as the main source of nTA.

The DIC variation is more complicated than the TA variation because the spatiotemporal variation in biological metabolism and vertical advection is larger and more significant than that of TA, in addition to the effect of CO<sub>2</sub> exchange with the atmosphere. Unlike the TA, the seasonal variations in the landwater supply were not consistent with those in the  
 270 time derivative (Figure 4e). This trend indicated that landwater supply was not the primary driver of DIC variation in Area A. The effect of oceanic CO<sub>2</sub> uptake was highly variable and unclear on a decadal scale. However, on a seasonal scale, it was more distinct, resulting in negative shifts in the summer residual terms and positive shifts in the winter residual terms." This seasonal variation indicated that the oceanic CO<sub>2</sub> uptake in Area A was larger than that in Area B in summer, and vice versa in winter. This was caused by the lower seawater fCO<sub>2</sub> in Area A during the summer season and higher wind velocity in  
 275 Area B during the winter season. Consequently, the residual term of nDIC indicated a strong and complex seasonal variation, which included a maximum in the winter and two minimums in spring and summer with a difference of  $100 \mu\text{mol kg}^{-1} \text{ year}^{-1}$ . Contrary to TA, DIC was affected by nutrient and organic matter loading from terrestrial sources, and was strongly affected by differences in biological metabolism between Areas A and B. For DIC, in contrast to TA, a significant vertical profile trend was observed (Text S1); consequently, some of the residual terms might have been influenced by vertical advection.

280 To quantify the effect of biological metabolism, the effects of horizontal and vertical advection were estimated based on the following assumptions: 1) the residual term for nTA ( $C_{res\_TA}$ ) was assumed to be equal to the horizontal advection term, based on the considerations that the effects of vertical advection and biological metabolism on nTA are negligible. 2) The horizontal advection term was proportional to  $dAB$  of nTA ( $dAB_{TA}$ ) and nDIC ( $dAB_{DIC}$ ). Several previous studies have used normalized values for the calculation of TA and DIC advection (Broecker and Peng, 1992; Keeling and Peng, 1995) and  
 285 have also proven their validity as an approximation (Robbins, 2001). Because the advection term is calculated as the product of concentration gradient and flow field, and the associated distance and flow velocity are the same at  $dAB_{TA}$  and  $dAB_{DIC}$ , it can be assumed that the horizontal advection effect on DIC ( $C_{adv\_DIC}$ ) can be estimated using the following equation:

$$C_{adv\_DIC} = K \frac{dAB_{DIC}}{D_{AB}}$$

$$C_{res\_TA} = K \frac{dAB_{TA}}{D_{AB}}$$

290  $C_{adv\_DIC} = C_{res\_TA} \cdot \frac{dAB_{DIC}}{dAB_{TA}} \quad (4)$

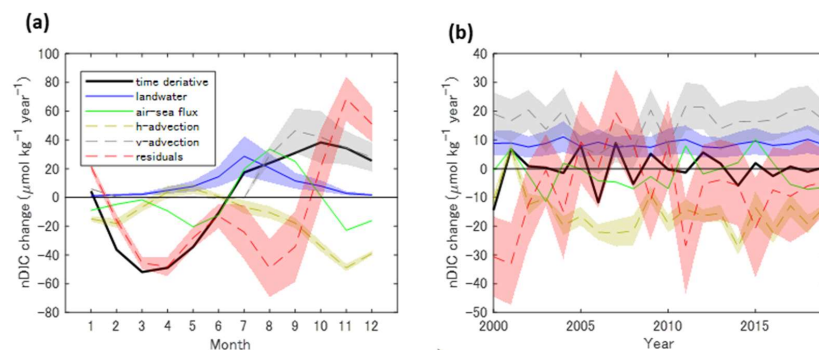


where,  $K$  and  $D_{AB}$  are the index values associated with the current field and horizontal distance between Areas A and B, respectively. These parameters were assumed to be the same for TA and DIC calculations. 3) Vertical advection for nDIC ( $C_{vadv\_DIC}$ ) was estimated from mixing with subsurface water when the mixed layer was deepened. Specifically, we used a simplified equation of the method of a previous study (Ishii et al., 2001).

$$295 \int C_{vadv\_DIC}(t)dt = \frac{\{\Delta nDIC(t+1)+\Delta nDIC(t)\}}{2} \times \frac{\{MLD(t+1)-MLD(t)\}}{\{\rho_{MLD(t+1)}\}} \\ \Delta nDIC(t) = \{nDIC(July, MLD(t)) - nDIC(t, MLD(t))\} \cdot \rho_{MLD(t)} \quad (5)$$

where,  $\Delta nDIC(t)$  is the difference between the average nDIC in July ( $nDIC(July)$ ) and the nDIC at time  $t$  at mixed layer depth ( $MLD(t)$ ) multiplied by the seawater density at  $MLD(t)$  ( $\rho_{MLD(t)}$ ). The nDIC profile at a depth below the mixed layer was assumed to be maintained at its average value in July; as the mixed layer deepened, the difference from the July profile was added to the nDIC in the mixed layer. The effect of vertical advection on nDIC was negligible when the mixed-layer depth did not change or became shallower. The details on the calculation of the nDIC profiles are provided in Text S1.

The effects of horizontal and vertical advection on nDIC are shown in Figure 6. However, due to the large error range in the vertical advection term for each time step (the median was 137%), only the monthly and annual averages are shown in the figure. The horizontal and vertical advection effects were identified mainly from autumn to winter with an annual mean value of  $-15.55 \pm 1.35 \mu\text{mol kg}^{-1} \text{ year}^{-1}$  and  $15.55 \pm 2.25 \mu\text{mol kg}^{-1} \text{ year}^{-1}$ , respectively (Ave  $\pm$  SE). Seasonally, the residual term had a maximum in the winter and two minimums in spring and summer, with an overall mean of  $-7.30 \pm 3.24 \mu\text{mol kg}^{-1} \text{ year}^{-1}$ .



310 **Figures 6. Temporal variations of nTA time derivative and related terms in Equation (2) (a): The monthly averages. (b): The yearly averages. The shaded areas of horizontal advection (h-advection) and vertical advection (v-advection) are the random error calculated using the error propagation (see Text S1). Therefore, unlike the error ranges of  $Sup_{hw}$ , these were reduced by  $10^{-0.5}$  or  $20^{-0.5}$  by monthly or yearly averaging, respectively.**



315 Although the above results were not definitive because of many assumptions and large error ranges, the fact that the final residual term on the decadal scale was almost negative supports the idea that Area A is likely under heterotrophic conditions within the mixed layer. The positive shift in the residual term before and after 2007 was due to the low vertical advection term caused by the small MLD during winter. The 2007 minimum SST in Area A (19.41 °C) was the highest of the overall annual minimum SST ( $17.71 \pm 0.66$  °C, Ave  $\pm$  SD), and thus the surface seawater mixing would be weaker than that in other years. Therefore, the residual term for this period does not necessarily indicate changes in biological metabolism. However, the high SST during winter suggests that the decomposition of biofixed carbon may be accelerated. Seasonally, the March-April minimum in the residual term was assumed to be the result of phytoplankton blooms in the open ocean area in Area A. Another minimum in July-August was assumed to be due to the primary production of phytoplankton and submerged aquatic vegetation under eutrophic conditions in the inner bays and near-shore areas. The winter maximum can be explained by the upwelling of organic matter and the decomposition of bio-fixed carbons within the mixed layer.

It should be noted that the residual term above includes the effects of the water CO<sub>2</sub> flux in near-shore areas. However, unlike the air-sea CO<sub>2</sub> flux in the ocean ( $C_{flux}$  in Equation (2)), the air-water CO<sub>2</sub> flux in near-shore areas is very difficult to quantify because observations of water fCO<sub>2</sub> and the physical regulating factor defined as “transfer velocity” (e.g., Wanninkhof, 2014) are limited. The estimation of this CO<sub>2</sub> flux varies widely among the existing studies. For example, global average models (Aufdenkamp et al., 2011; Tranvik et al., 2009) have estimated that approximately half of the carbon supply from land is released into the atmosphere via the air-water CO<sub>2</sub> flux in near-shore areas. However, the inner bays affected by landwater in this study showed a trend in atmospheric CO<sub>2</sub> absorption (Tokoro et al., 2021), that is unlikely to follow the global average trend. Therefore, enhanced observation and analysis of atmospheric CO<sub>2</sub> exchange in nearshore areas is essential for a more accurate assessment of the residual term as an indicator of biological metabolism.

335 Despite Area A having a higher nDIC than Area B (Figure 3), seawater fCO<sub>2</sub> in Area A tended to be lower than in Area B ( $-3.61 \pm 0.70$  μatm). This was mainly because of the lower SST and higher nTA in Area A than those in Area B (Figure 5). The low SST can likely be attributed to landwater, which is mainly supplied by snowmelt and rainfall from the mountains and highlands and therefore tends to have lower original water temperatures. In particular, the short flow paths of Japanese rivers can likely limit the effects of heating due to solar radiation and other factors. The three inner bays with strong river influence had lower average water temperature (18.66–19.23 °C, Tokoro et al., 2021) than areas A (22.02 °C) and B (22.86 °C), which support our assumption. The decrease in seawater fCO<sub>2</sub> peaked in the summer ( $-15.90 \pm 4.72$  μatm from July to September), when the decrease in nDIC due to biological metabolism and the increase in nTA due to river supply coincided. However, this decreasing in seawater fCO<sub>2</sub> had little effect on annual oceanic CO<sub>2</sub> uptake in Area A. Compared to the hypothetical case where landwater did not affect seawater fCO<sub>2</sub> (seawater fCO<sub>2</sub> in Area A were the same as that in Area B), the change in air-sea CO<sub>2</sub> flux would be similar ( $0.00 \pm 0.33$  mol m<sup>-2</sup> year<sup>-1</sup>). This was because the decrease in air-sea CO<sub>2</sub> flux in summer almost offsets the increase in winter. Although the increase in seawater fCO<sub>2</sub> in winter was smaller than the decrease in summer, the air-sea CO<sub>2</sub> fluxes in summer and winter were coincidentally balanced, owing to higher wind speeds in winter.



For  $\Omega_{\text{cal}}$ , seawater in Area A was notably more acidified than in the surrounding sea area, based on a 20-year average (-  
350  $0.13 \pm 0.01$ ). The impact on coastal acidification was particularly significant in winter, with an average decrease of  $-0.25$   
( $5.33$  to  $5.08$ ).  $n\text{TA}$  was only mitigation factor for coastal acidification among the explanatory variables, and reduced  
acidification due to other factors to 65% ( $-0.20$  to  $-0.13$ ). This coastal acidification was found to be progressing, with  $dAB$  of  
 $\Omega_{\text{cal}}$  decreasing by  $-0.52 \pm 0.14$  per decade. This can be attributed to an increasing trend in  $dAB$  of  $n\text{DIC}$  ( $0.32 \pm 0.08 \mu\text{mol}$   
 $\text{kg}^{-1} \text{year}^{-1}$ ) due to the trend of increasing precipitation in Japan.

355

## 5. Conclusions

In this study, we identified areas affected by landwater in the Northwest Pacific Ocean by using statistically processed  
observational data. We also evaluated the contribution of landwater to oceanic  $\text{CO}_2$  uptake and coastal acidification by  
comparing the TA and DIC values in the sea area affected by landwater and surrounding sea areas.

360 The Area A affected by landwater (Area A) was within 246.67 km of mainland Japan and, to some extent, along the  
Kuroshio axis. This area was consistent with the low-SSS area of low SSS on the Pacific coast of Japan. In addition, the  
range increased to 353.61 km during the period when the Kuroshio Current meandered south, indicating that the Kuroshio  
Current path influences the spread of landwater.

Both  $n\text{TA}$  and  $n\text{DIC}$  were higher in surrounding sea in Area A. The main source of TA was landwater in summer, which was  
365 balanced by a decrease due to horizontal advection in autumn and winter. The DIC flows were more complex than the TA  
flows and were more strongly affected by a residual term than by the landwater supply. The contribution of biological  
metabolism is expected to be more influential on the residual term after excluding the horizontal and vertical advection  
effects. Biological metabolism showed a maximum in winter and two minima in spring and summer. The annual mean  
suggests heterotrophic conditions within the mixed layer in Area A. In any case, because the air-water  $\text{CO}_2$  flux in near-shore  
370 areas is still difficult to estimate, a more thorough quantification of DIC flow in relation to landwater needs to be considered.

Seawater  $f\text{CO}_2$  in Area A decreased mainly in summer because of the supplied landwater, which has low-temperature  
water with high  $n\text{TA}$ . However, landwater supply was found to have virtually no effect on oceanic  $\text{CO}_2$  uptake at an annual  
scale. This is because  $\text{CO}_2$  emission was enhanced by strong wind speeds in winter, in addition to the relatively small  
increase in seawater  $f\text{CO}_2$  in winter. The change in the air-sea  $\text{CO}_2$  flux in winter was coincidentally balanced by the change  
375 in summer, and the annual average was almost zero. Although acidification progressed more in Area A than in the  
surrounding sea area, the supply of TA by landwater mitigated the acidification to 65%. However, an increase in  
precipitation may have led to increases in  $n\text{DIC}$  and acidification in Area A.

This study makes a significant contribution to the analysis of carbon flows in the boundary seawater between terrestrial  
and oceanic areas because the quantification of carbon flows in these areas is often uncertain in space and time. Enhancing  
380 the observational data allows the results to be spatially extended to larger regional or global scales. The analysis results are





expected to have a smaller error range owing to the high spatiotemporal resolution of the vertical profiles of the carbonate data and air-water CO<sub>2</sub> flux data in near-shore areas.

#### Data Availability

385 The SSS, SST, and fCO<sub>2</sub> in air and seawater datasets are available in the SOCAT database (Pfeil et al., 2013; Bakker et al., 2016, <https://socat.info/index.php/data-access/>). The TA and DIC data were available from the GLODAP database version 2.2020 (Key et al., 2015; Olsen et al., 2016; Olsen, 2020, <https://glodap.info/>). Wind speed data were obtained from the CCMP database (version 2.0) (Atlas et al., 2011; Mears et al., 2019; <https://data.remss.com/ccmp/v02.0/>). The river flow datasets were obtained from the Water Information System of the Ministry of Land, Infrastructure, Transport, and Tourism of  
390 Japan (<http://www1.river.go.jp/>). Vertical water temperature datasets for calculating MLD were obtained from the JCOPE2M dataset (Miyazawa et al., 2017, 2019, . <https://www.jamstec.go.jp/jcope/htdocs/distribution/>).

#### Author Contribution

TT designed the study and wrote the first draft on the manuscript. SN, ST, SS, SD, KE, MI, NK, TO, KT, and YN supplied  
395 and managed data for SOCAT and GLODAP. SN supported data processing. All authors contributed to manuscript writing and proofing.

#### Competing interests

The contact author has declared that none of the authors have any competing interests.

400

#### Acknowledgments

We appreciate the cooperation of Toyofuji Shipping Co. and Kagoshima Senpaku Co. in the NIES VOS program. We also thank the captains and crews of M/S Pyxis, M/S New Century 2, M/S Trans Future 5, R/V Mirai, R/V Hakuho-maru, R/V Keifu-maru, R/V Ryofu-maru, R/V Wakataka-maru, and R/V Soyo-maru. This research was financially supported by the  
405 Global Environmental Research Coordination System, Ministry of the Environment, Japan (grant numbers MOE1751 and MOE 2252) and CREST, Japan Science and Technology Agency (grant number JPMJCR23J4).

#### References

Andreev, A. G. and Pavlova, G. Y.: Marginal Seas, in: Carbon and nutrient fluxes in continental margins, edited  
410 by Liu, K. K., Atkinson, L., Quiñones, R., and Talaue-McManus, L., Springer, New York, 395–406, 2009.



- Atlas, R., Hoffman, R. N., Ardizzone, J., Leidner, S. M., Jusem, J. C., Smith, D. K., and Gombos, D.: A Cross-calibrated Multiplatform Ocean Surface Wind Velocity Product for Meteorological and Oceanographic Applications, *Bull. Amer. Meteor. Soc.*, 92, 157–174. <https://doi.org/10.1175/2010BAMS2946.1>, 2011.
- 415
- Aufdenkampe, A. K., Mayorga, E., Raymond, P. A., Melack, J. M., Doney, S. C., Alin, S. R., Aalto, R. E., and Yoo, K.: Riverine coupling of biogeochemical cycles between land, oceans, and atmosphere, *Front. Ecol. Environ.*, 9, 53–60. <https://doi.org/10.1890/100014>, 2011.
- 420 Bakker, D. C. E., Pfeil, B., Landa, C. S., Metzl, N., O'Brien, K. M., Olsen, A., Smith, K., Cosca, C., Harasawa, S., Jones, S. D., Nakaoka, S., Nojiri, Y., Schuster, U., Steinhoff, T., Sweeney, C., Takahashi, T., Tilbrook, B., Wada, C., Wanninkhof, R., Alin, S. R., Balestrini, C. F., Barbero, L., Bates, N. R., Bianchi, A. A., Bonou, F., Boutin, J., Bozec, Y., Burger, E. F., Cai, W. J., Castle, R. D., Chen, L., Chierici, M., Currie, K., Evans, W., Featherstone, C., Feely, R. A., Fransson, A., Goyet, C., Greenwood, N., Gregor, L., Hankin, S., Hardman-
- 425 Mountford, N. J., Harlay, J., Hauck, J., Hoppema, M., Humphreys, M. P., Hunt, C. W., Huss, B., Ibáñez, J. S. P., Johannessen, T., Keeling, R., Kitidis, V., Körtzinger, A., Kozyr, A., Krasakopoulou, E., Kuwata, A., Landschützer, P., Lauvset, S. K., Lefèvre, N., Lo Monaco, C., Manke, A., Mathis, J. T., Merlivat, L., Millero, F. J., Monteiro, P. M. S., Munro, D. R., Murata, A., Newberger, T., Omar, A. M., Ono, T., Paterson, K., Pearce, D., Pierrot, D., Robbins, L. L., Saito, S., Salisbury, J., Schlitzer, R., Schneider, B., Schweitzer, R., Sieger, R.,
- 430 Skjelvan, I., Sullivan, K. F., Sutherland, S. C., Sutton, A. J., Tadokoro, K., Telszewski, M., Tuma, M., van Heuven, S. M. A. C., Vandemark, D., Ward, B., Watson, A. J., and Xu, S.: A multi-decade record of high-quality  $f\text{CO}_2$  data in version 3 of the Surface Ocean  $\text{CO}_2$  Atlas (SOCAT), *Earth Syst. Sci. Data*, 8, 383–413. <https://doi.org/10.5194/essd-8-383-2016>, 2016.
- 435 Bauer, J. E., Cai, W. J., Raymond, P. A., Bianchi, T. S., Hopkinson, C. S., and Regnier, P. A. G.: The changing carbon cycle of the coastal ocean, *Nature*, 504, 61–70. <https://doi.org/10.1038/nature12857>, 2013.
- Borges, A. V., Delille, B., and Frankignoulle, M.: Budgeting sinks and sources of  $\text{CO}_2$  in the coastal ocean: Diversity of ecosystems counts, *Geophys. Res. Lett.*, 32, L14601. <https://doi.org/10.1029/2005GL023053>, 2005.
- 440 Brewer, P. G. and Goldman, J. C.: Alkalinity changes generated by phytoplankton growth, *Limnol. Oceanogr.*, 21, 108–117. <https://doi.org/10.4319/lo.1976.21.1.0108>, 1976.



- Broecker, W. S. and Peng, T. H.: Tracers in the sea, Eldigio Press, New York, 1982.  
445
- Broecker, W. S. and Peng, T. H.: Interhemispheric transport of carbon dioxide by ocean circulation, *Nature*, 356, 587–589. <https://doi.org/10.1038/356587a0>, 1992.
- Cai, W. J.: Estuarine and coastal ocean carbon paradox: CO<sub>2</sub> sinks or sites of terrestrial carbon incineration? *Ann. Rev. Mar. Sci.*, 3, 123–145. <https://doi.org/10.1146/annurev-marine-120709-142723>, 2011.  
450
- Carstensen, J. and Duarte, C. M.: Drivers of pH variability in coastal ecosystems, *Environ. Sci. Technol.*, 53, 4020–4029. <https://doi.org/10.1021/acs.est.8b03655>, 2019.
- 455 Chen, C. T. A. and Borges, A. V.: Reconciling opposing views on carbon cycling in the coastal ocean: Continental shelves as sinks and near-shore ecosystems as sources of atmospheric CO<sub>2</sub>, *Deep Sea Research Part II: Topical Studies in Oceanography*, 56, 578–590. <https://doi.org/10.1016/j.dsr2.2009.01.001>, 2009.
- Chen, C. T. A., Huang, T. H., Chen, Y. C., Bai, Y., He, X., and Kang, Y.: Air-sea exchanges of CO<sub>2</sub> in the  
460 world's coastal seas, *Biogeosciences*, 10, 6509–6544. <https://doi.org/10.5194/bg-10-6509-2013>, 2013.
- de Boyer Montégut, C., Madec, G., Fischer, A. S., Lazar, A., and Iudicone, D.: Mixed layer depth over the global ocean: An examination of profile data and a profile-based climatology, *J. Geophys. Res.*, 109. <https://doi.org/10.1029/2004JC002378>, 2004.  
465
- Denbo, D. W. and Allen, J. S.: Rotary empirical orthogonal function analysis of currents near the Oregon Coast, *J. Phys. Oceanogr.*, 14, 35–46. [https://doi.org/10.1175/1520-0485\(1984\)014<0035:REOFAO>2.0.CO;2](https://doi.org/10.1175/1520-0485(1984)014<0035:REOFAO>2.0.CO;2), 1984.
- Duarte, C. M., Hendriks, I. E., Moore, T. S., Olsen, Y. S., Steckbauer, A., Ramajo, L., Carstensen, J., Trotter, J.  
470 A., and McCulloch, M.: Is ocean acidification an open-ocean syndrome? Understanding anthropogenic impacts on seawater pH, *Estuaries Coasts*, 36, 221–236. <https://doi.org/10.1007/s12237-013-9594-3>, 2013.



- 475 Fitzer, S. C., Torres Gabarda, S. T., Daly, L., Hughes, B., Dove, M., O'Connor, W., Potts, J., Scanes, P., and  
Byrne, M.: Coastal acidification impacts on shell mineral structure of bivalve mollusks, *Ecol. Evol.*, 8, 8973–  
8984. <https://doi.org/10.1002/ecc3.4416>, 2018.
- Friis, K., Körtzinger, A., and Wallace, D. W. R.: The salinity normalization of marine inorganic carbon chemistry  
data, *Geophys. Res. Lett.*, 30. <https://doi.org/10.1029/2002GL015898>, 2003.
- 480 Holte, J. and Talley, L.: A new algorithm for finding mixed layer depths with applications to argo data and  
Subantarctic mode water formation, *J. Atmos. Ocean. Technol.*, 26, 1920–1939.  
<https://doi.org/10.1175/2009JTECHO543.1>, 2009.
- Hopkins, J. and Balch, W. M.: A new approach to estimating coccolithophore calcification rates from space, *JGR*  
485 *Biogeosciences.*, 123, 1447–1459. <https://doi.org/10.1002/2017JG004235>, 2018.
- Inoue, H. Y., Matsueda, H., Ishii, M., Fushimi, K., Hirota, M., Asanuma, I., and Takasugi, Y.: Long-term trend of  
the partial-pressure of carbon-dioxide ( $p\text{CO}_2$ ) in surface waters of the western North Pacific, 1984–1993, *Tellus*  
B., 47, 391–413. <https://doi.org/10.1034/j.1600-0889.47.issue4.2.x>, 1995.
- 490 Ishii, M., Inoue, H. Y., Matsueda, H., Saito, S., Fushimi, K., Nemoto, K., Yano, T., Nagai, H., and Midorikawa,  
T.: Seasonal variation in total inorganic carbon and its controlling processes in surface waters of the western  
North Pacific subtropical gyre, *Mar. Chem.*, 75, 17–32. [https://doi.org/10.1016/S0304-4203\(01\)00023-8](https://doi.org/10.1016/S0304-4203(01)00023-8), 2001.
- 495 Kawabe, M.: Sea level variations at the Izu Islands and typical stable paths of the Kuroshio, *J. Ocean. Soc. Jpn.*,  
41, 307–326. <https://doi.org/10.1007/BF02109238>, 1985.
- Keeling, R. and Peng, T. H.: Transport of heat,  $\text{CO}_2$ , and  $\text{O}_2$  by the Atlantic's thermohaline circulation, *Phil.*  
*Trans. R. Soc. Lond. B*, 348, 133–142. <https://doi.org/10.1098/rstb.1995.0055>, 1995.
- 500 Kessouri, F., McWilliams, J. C., Bianchi, D., Sutula, M., Renault, L., Deutsch, C., Feely, R. A., McLaughlin, K.,  
Ho, M., Howard, E. M., Bednaršek, N., Damien, P., Molemaker, J., and Weisberg, S. B.: Coastal eutrophication



drives acidification, oxygen loss, and ecosystem change in a major oceanic upwelling system, *Proc. Natl Acad. Sci. U. S. A.*, 118. <https://doi.org/10.1073/pnas.2018856118>, 2021.

505

Key, R. M., Olsen, A., van Heuven, S., Lauvset, S. K., Velo, A., Lin, X., Schirnack, C., Kozyr, A., Tanhua, T., Hoppema, M., Jutterström, S., Steinfeldt, R., Jeansson, E., Ishii, M., Perez, F. F., and Suzuki, T.: Global ocean data analysis project, version 2, (GLODAPv2), Oak Ridge National Laboratory/CDIAC-162, NDP-093, Carbon Dioxide Information Analysis Center, Oak Ridge National Laboratory, United States Department of Energy, Oak Ridge, TN. [https://doi.org/10.3334/CDIAC/OTG.NDP093\\_GLODAPv2](https://doi.org/10.3334/CDIAC/OTG.NDP093_GLODAPv2). [dataset] 2015.

510

Killick, R., Fearnhead, P., and Eckley, I. A.: Optimal detection of changepoints with a linear computational cost, *J. Am. Stat. Assoc.*, 107, 1590–1598. <https://doi.org/10.1080/01621459.2012.737745>, 2012.

515

Kitamura, T., Nakano, T., and Sugimoto, S.: Decadal variations in mixed layer salinity in the Kuroshio Extension recirculation gyre region: Influence of precipitation during the warm season, *J. Oceanogr.*, 72, 167–175. <https://doi.org/10.1007/s10872-015-0317-1>, 2016.

520

Krumhardt, K. M., Lovenduski, N. S., Long, M. C., Levy, M., Lindsay, K., Moore, J. K., and Nissen, C.: Coccolithophore growth and calcification in an acidified ocean: Insights from community earth system model simulations, *J. Adv. Model. Earth Syst.*, 11, 1418–1437. <https://doi.org/10.1029/2018MS001483>, 2019.

525

Lee, K., Tong, L. T., Millero, F. J., Sabine, C. L., Dickson, A. G., Goyet, C., Park, G. H., Wanninkhof, R., Feely, R. A., and Key, R. M.: Global relationships of total alkalinity with salinity and temperature in surface waters of the world's oceans, *Geophys. Res. Lett.*, 33. <https://doi.org/10.1029/2006GL027207>, 2006.

530

Lehmann, N., Lantuit, H., Böttcher, M. E., Hartmann, J., Eulenburg, A., and Thomas, H.: Alkalinity generation from carbonate weathering in a silicate-dominated headwater catchment at Iskorasfjellet, northern Norway, *Biogeosciences*, 20, 3459–3479. <https://doi.org/10.5194/bg-20-3459-2023>, 2023.

Mears, C. A., Scott, J., Wentz, F. J., Ricciardulli, L., Leidner, S. M., Hoffman, R., and Atlas, R.: A near-real-time version of the Cross-Calibrated Multiplatform (CCMP) ocean surface wind velocity data set, *JGR Oceans*, 124, 6997–7010. <https://doi.org/10.1029/2019JC015367> [dataset], 2019.



- 535 Millero, F. J., Lee, K., and Roche, M.: Distribution of alkalinity in the surface waters of the major oceans, *Mar. Chem.*, 60, 111–130. [https://doi.org/10.1016/S0304-4203\(97\)00084-4](https://doi.org/10.1016/S0304-4203(97)00084-4), 1998.
- Miyama, T., Minobe, S., and Goto, H.: Marine heatwave of sea surface temperature of the Oyashio region in summer in 2010–2016, *Front. Mar. Sci.*, 7. <https://doi.org/10.3389/fmars.2020.576240>, 2021.
- 540 Miyazawa, Y., Kuwano-Yoshida, A., Doi, T., Nishikawa, H., Narazaki, T., Fukuoka, T., and Sato, K.: Temperature profiling measurements by sea turtles improve ocean state estimation in the Kuroshio-Oyashio Confluence region, *Ocean Dyn.*, 69, 267–282. <https://doi.org/10.1007/s10236-018-1238-5> [dataset], 2019.
- 545 Miyazawa, Y., Varlamov, S. M., Miyama, T., Guo, X. Y., Hihara, T., Kiyomatsu, K., Kachi, M., Kurihara, Y., and Murakami, H.: Assimilation of high-resolution sea surface temperature data into an operational nowcast/forecast system around Japan using a multi-scale three-dimensional variational scheme, *Ocean Dyn.*, 67, 713–728. <https://doi.org/10.1007/s10236-017-1056-1> [dataset], 2017.
- 550 Murata, A. M., Kaneko, I., Nemoto, K., Fushimi, K., and Hirota, M.: Spatial and temporal variations of surface seawater  $f(\text{CO}_2)$  in the Kuroshio off Japan, *Mar. Chem.*, 59, 189–200. [https://doi.org/10.1016/S0304-4203\(97\)00096-0](https://doi.org/10.1016/S0304-4203(97)00096-0), 1998.
- Olsen, A., Key, R. M., van Heuven, S., Lauvset, S. K., Velo, A., Lin, X. H., Schirnack, C., Kozyr, A., Tanhua, T.,  
555 Hoppema, M., Jutterström, S., Steinfeldt, R., Jeansson, E., Ishii, M., Pérez, F. F., and Suzuki, T.: The Global Ocean Data Analysis Project version 2 (GLODAPv2) - An internally consistent data product for the world ocean, *Earth Syst. Sci. Data*, 8, 297–323. <https://doi.org/10.5194/essd-8-297-2016> [dataset], 2016.
- Olsen, A., Lange, N., Key, R. M., Tanhua, T., Bittig, H. C., Kozyr, A., Álvarez, M., Azetsu-Scott, K., Becker, S.,  
560 Brown, P. J., Carter, B. R., Cotrim da Cunha, L., Feely, R. A., van Heuven, S., Hoppema, M., Ishii, M., Jeansson, E., Jutterström, S., Landa, C. S., Lauvset, S. K., Michaelis, P., Murata, A., Pérez, F. F., Pfeil, B., Schirnack, C., Steinfeldt, R., Suzuki, T., Tilbrook, B., Velo, A., Wanninkhof, R., and Woosley, R. J.: An updated version of the global interior ocean biogeochemical data product, GLODAPv2.2020., *Earth Syst. Sci. Data*, 12, 3653–3678. <https://doi.org/10.5194/essd-12-3653-2020>, 2020.



565

Passow, U. and Carlson, C. A.: The biological pump in a high CO<sub>2</sub> world, *Mar. Ecol. Prog. Ser.*, 470, 249–271.

<https://doi.org/10.3354/meps09985>, 2012.

- Pfeil, B., Olsen, A., Bakker, D. C. E., Hankin, S., Koyuk, H., Kozyr, A., Malczyk, J., Manke, A., Metzl, N.,  
570 Sabine, C. L., Akl, J., Alin, S. R., Bates, N., Bellerby, R. G. J., Borges, A., Boutin, J., Brown, P. J., Cai, W. J.,  
Chavez, F. P., Chen, A., Cosca, C., Fassbender, A. J., Feely, R. A., González-Dávila, M., Goyet, C., Hales, B.,  
Hardman-Mountford, N., Heinze, C., Hood, M., Hoppema, M., Hunt, C. W., Hydes, D., Ishii, M., Johannessen,  
T., Jones, S. D., Key, R. M., Körtzinger, A., Landschützer, P., Lauvset, S. K., Lefèvre, N., Lenton, A., Lourantou,  
A., Merlivat, L., Midorikawa, T., Mintrop, L., Miyazaki, C., Murata, A., Nakadate, A., Nakano, Y., Nakaoka, S.,  
575 Nojiri, Y., Omar, A. M., Padin, X. A., Park, G. H., Paterson, K., Perez, F. F., Pierrot, D., Poisson, A., Ríos, A. F.,  
Santana-Casiano, J. M., Salisbury, J., Sarma, V. V. S. S., Schlitzer, R., Schneider, B., Schuster, U., Sieger, R.,  
Skjelvan, I., Steinhoff, T., Suzuki, T., Takahashi, T., Tedesco, K., Telszewski, M., Thomas, H., Tilbrook, B.,  
Tjiputra, J., Vandemark, D., Veness, T., Wanninkhof, R., Watson, A. J., Weiss, R., Wong, C. S., and Yoshikawa-  
Inoue, H.: A uniform, quality controlled Surface Ocean CO<sub>2</sub> Atlas (SOCAT), *Earth Syst. Sci. Data*, 5, 125–143.  
580 <https://doi.org/10.5194/essd-5-125-2013>, 2013.

Rassmann, J., Lansard, B., Pozzato, L., and Rabouille, C.: Carbonate chemistry in sediment porewaters of the  
Rhône River delta driven by early diagenesis (northwestern Mediterranean), *Biogeosciences*, 13, 5379–5394.

<https://doi.org/10.5194/bg-13-5379-2016>, 2016.

585

- Regnier, P., Friedlingstein, P., Ciais, P., Mackenzie, F. T., Gruber, N., Janssens, I. A., Laruelle, G. G., Lauerwald,  
R., Luyssaert, S., Andersson, A. J., Arndt, S., Arnosti, C., Borges, A. V., Dale, A. W., Gallego-Sala, A., Goddérís,  
Y., Goossens, N., Hartmann, J., Heinze, C., Ilyina, T., Joos, F., LaRowe, D. E., Leifeld, J., Meysman, F. J. R.,  
Munhoven, G., Raymond, P. A., Spahni, R., Suntharalingam, P., and Thullner, M.: Anthropogenic perturbation of  
590 the carbon fluxes from land to ocean, *Nature Geosci.*, 6, 597–607. <https://doi.org/10.1038/Ngeo1830>, 2013.

Regnier, P., Resplandy, L., Najjar, R. G., and Ciais, P.: The land-to-ocean loops of the global carbon cycle,

*Nature*, 603, 401–410. <https://doi.org/10.1038/s41586-021-04339-9>, 2022.



- 595 Robbins, P. E.: Oceanic carbon transport carried by freshwater divergence: Are salinity normalizations useful? *J. Geophys. Res.*, 106, 30939–30946. <https://doi.org/10.1029/2000JC000451>, 2001.
- Sugimoto, S., Takahashi, N., and Hanawa, K.: Marked freshening of North Pacific subtropical mode water in 2009 and 2010: Influence of freshwater supply in the 2008 warm season, *Geophys. Res. Lett.*, 40, 3102–3105.
- 600 <https://doi.org/10.1002/grl.50600>, 2013.
- Taguchi, F., Fujiwara, T., Yamada, Y., Fujita, K., and Sugiyama, M.: Alkalinity in coastal seas around Japan, *Bull. Coast. Oceanogr.*, 47, 71–75, 2009.
- 605 Takahashi, T., Sutherland, S. C., Sweeney, C., Poisson, A., Metzl, N., Tilbrook, B., Bates, N., Wanninkhof, R., Feely, R. A., Sabine, C., Olafsson, J., and Nojiri, Y.: Global sea-air CO<sub>2</sub> flux based on climatological surface ocean pCO<sub>2</sub>, and seasonal biological and temperature effects, *Deep Sea Research Part II: Topical Studies in Oceanography*, 49, 1601–1622. [https://doi.org/10.1016/S0967-0645\(02\)00003-6](https://doi.org/10.1016/S0967-0645(02)00003-6), 2002.
- 610 Takahashi, T., Sutherland, S. C., Wanninkhof, R., Sweeney, C., Feely, R. A., Chipman, D. W., Hales, B., Friederich, G., Chavez, F., Sabine, C., Watson, A., Bakker, D. C. E., Schuster, U., Metzl, N., Yoshikawa-Inoue, H., Ishii, M., Midorikawa, T., Nojiri, Y., Körtzinger, A., Steinhoff, T., Hoppema, M., Olafsson, J., Arnarson, T. S., Tilbrook, B., Johannessen, T., Olsen, A., Bellerby, R., Wong, C. S., Delille, B., Bates, N. R., and de Baar, H. J. W.: Climatological mean and decadal change in surface ocean pCO<sub>2</sub>, and net sea-air CO<sub>2</sub> flux over the global
- 615 oceans, *Deep Sea Research Part II: Topical Studies in Oceanography*, 56, 554–577. <https://doi.org/10.1016/j.dsr2.2008.12.009>, 2009.
- Takamura, T. R., Inoue, H. Y., Midorikawa, T., Ishii, M., and Nojiri, Y.: Seasonal and interannual variations in pCO<sub>2</sub>(sea) and air-sea CO<sub>2</sub> fluxes in midlatitudes of the western and eastern North Pacific during 1999–2006: Recent results utilizing voluntary observation ships, *J. Meteorol. Soc. Jpn.*, 88, 883–898. <https://doi.org/10.2151/jmsj.2010-602>, 2010.
- Takatani, Y., Enyo, K., Iida, Y., Kojima, A., Nakano, T., Sasano, D., Kosugi, N., Midorikawa, T., Suzuki, T., and Ishii, M.: Relationships between total alkalinity in surface water and sea surface dynamic height in the Pacific
- 625 Ocean, *J. Geophys. Res. Oceans*, 119, 2806–2814. <https://doi.org/10.1002/2013JC009739>, 2014.





Tokoro, T., Nakaoka, S., Takao, S., Kuwae, T., Kubo, A., Endo, T., and Nojiri, Y.: Contribution of biological effects to carbonate-system variations and the air-water CO<sub>2</sub> flux in urbanized bays in Japan, *JGR Oceans*, 126. <https://doi.org/10.1029/2020JC016974>, 2021.

630

Tokoro, T., Nakaoka, S., Takao, S., Saito, S., Sasano, D., Enyo, K., Ishii, M., Kosugi, N., and Nojiri, Y.: Statistical analysis of spatiotemporal variations of air-sea CO<sub>2</sub> fluxes in the Kuroshio region, *JGR Oceans*, 128. <https://doi.org/10.1029/2023JC019762>, 2023.

635 Tranvik, L. J., Downing, J. A., Cotner, J. B., Loiselle, S. A., Striegl, R. G., Ballatore, T. J., Dillon, P., Finlay, K., Fortino, K., Knoll, L. B., Kortelainen, P. L., Kutser, T., Larsen, S., Laurion, I., Leech, D. M., McCallister, S. L., McKnight, D. M., Melack, J. M., Overholt, E., Porter, J. A., Prairie, Y., Renwick, W. H., Roland, F., Sherman, B. S., Schindler, D. W., Sobek, S., Tremblay, A., Vanni, M. J., Verschoor, A. M., von Wachenfeldt, E., and Weyhenmeyer, G. A.: Lakes and reservoirs as regulators of carbon cycling and climate, *Limnol. Oceanogr.*, 54, 2298–2314. [https://doi.org/10.4319/lo.2009.54.6\\_part\\_2.2298](https://doi.org/10.4319/lo.2009.54.6_part_2.2298), 2009.

Wallace, R. B., Baumann, H., Grear, J. S., Aller, R. C., and Gobler, C. J.: Coastal Ocean acidification: The other eutrophication problem, *Estuarine Coast. Shelf Sci.*, 148, 1–13. <https://doi.org/10.1016/j.ecss.2014.05.027>, 2014.

645 Wanninkhof, R.: Relationship between wind speed and gas exchange over the ocean revisited, *Limnol. Oceanogr. Methods*, 12, 351–362. <https://doi.org/10.4319/lom.2014.12.351>, 2014.

Wold, S., Sjöström, M., and Eriksson, L.: PLS-regression: A basic tool of chemometrics, *Chemom. Intell. Lab. Syst.*, 58, 109–130. [https://doi.org/10.1016/S0169-7439\(01\)00155-1](https://doi.org/10.1016/S0169-7439(01)00155-1), 2001.

650

Yoshikawa-Inoue, H., Midorikawa, T., and Takamura, T. R.: Temporal and spatial variations in carbonate system and air-sea CO<sub>2</sub> flux in the Kuroshio and Kuroshio Extension, in: *Western Pacific air-sea interaction study*, edited by Uematsu, M., Yokouchi, Y., Watanabe, Y. W., Takebe, S., and Yamanaka, Y., Terra Publishing, Tokyo, 2014. <https://doi.org/10.5047/w-pass.a02.004>.

655

<https://doi.org/10.5194/egusphere-2024-3792>

Preprint. Discussion started: 10 January 2025

© Author(s) 2025. CC BY 4.0 License.



Zeebe, R. E. and Wolf-Gladrow, D.: CO<sub>2</sub> in seawater: Equilibrium, kinetics and isotopes, Elsevier Science, Amsterdam, 2001.